CHEMICAL ENGINEERING TRANSACTIONS
VOL. 76, 2019
A publication of AIDIC
The Italian Association of Chemical Engineering
Online at www.aidic.it/cet
Guest Editors: Petar S. Varbanov, Timothy G. Walmsley, Jiří J. Klemeš, Panos Seferlis

ISBN 978-88-95608-73-0; **ISSN** 2283-9216
DOI: 10.3303/CET1976015

Computational Method Study on Drag Coefficient of Butterfly Porous Fence

Zhenya Duan[a], Zhujun Lan[a], Jin Su[d], Kai Wang[a], Chi Zhou[a,b], Junmei Zhang[c,*]

[a]Electromechanical Engineering College, Qingdao University of Science and Technology, Qingdao, China
[b]Shanghai Turing Info Technology Co., Ltd, Shanghai, China
[c]College of Chemical Engineering, Qingdao University of Science and Technology, Qingdao, China
[d]Qingdao Changlong Power Equipment Co., Ltd, Qingdao, China
qust_zyduan@163.com

To study the drag coefficient of butterfly porous fence, this study proposes the computational model of butterfly porous fence based on the wind tunnel experiment. Effects of wind speed, porosity and hole diameter on the drag coefficient of the butterfly porous fence are investigated through the ANSYS Fluent. Under different wind speeds, the measurement results of the flow field behind the porous fence by the micro-particle image velocimetry (PIV) technology are found to be in good agreement with the numerical simulation. The numerical model can be considered correct and the simulation method is reasonable. Through the analysis of the simulation, research groups obtained some conclusions. Wind speed has almost no effect on drag coefficient when the maximum wind speed is over 10.0 m/s. The drag coefficient of the butterfly porous fence decreases gradually with the increase of porosity. Based on the simulation, the formula is established among drag coefficient, porosity and hole diameter when **d** is 6.6 mm ~ 9.5 mm. The research provides some theoretical basis for the butterfly porous fence engineering design. At the same time, it can effectively suppress dust diffusion to lighten the pollution of air.

1. Introduction

It was easy to produce dust pollution in open coal yards. These dusts could cause serious air pollution (Duan et al., 2017). Xu et al. (2010) had determined the drag coefficient of porous fence. He studied the drag coefficient of butterfly porous fence by means of pressure measurement and force measurement, which obtained the linear expression of the drag coefficient of the porous fence under different aperture. Chen et al. (2015) used CFD（computational fluid dynamics) to carry out numerical simulation research on diversion porous fence. Under certain conditions, the difference of wind load was small between two kinds of porous fence. Wind load increases quadratically with the wind speed.

By analyzing drag coefficients, research groups could quantitatively study the force of the porous fence. Briassoulis et al. (2010) used the elevated plate as the research object. He carried out numerical simulation and actual measurement on the drag coefficient of the elevated plate. The results showed that the drag coefficient could be an effective measure on the aerodynamic behavior of the open stencil.

Zhou (2017) studied on the drag coefficient of flat porous fence. Formula for the drag coefficient of the porous fence were summarized. According to the research of Xu et al. (2017), a butterfly porous fence model was established. ANSYS Fluent (Han, 2009) and wind tunnel experiment were used to study the drag coefficient of a butterfly porous fence (Ferreira et al., 2011).

Wind load should be considered in the design of butterfly porous fence. It was related to drag coefficient, but there were few theoretical studies at present, which restricts the popularization of butterfly porous fence. Research groups introduce butterfly porous fence model and numerical simulation. Then, results of PIV and numerical simulation were compared. Finally, results and discussion were obtained in this paper. The formula for the drag coefficient of a butterfly porous fence were summarized. The research provided some theoretical basis for the butterfly porous fence engineering design. At the same time, it can effectively suppress dust diffusion, to lighten the pollution of air.

Paper Received: 07/03/2019; Revised: 30/04/2019; Accepted: 06/05/2019
Please cite this article as: Duan Z., Lan Z., Su J., Wang K., Zhou C., Zhang J., 2019, Computational Method Study on Drag Coefficient of Butterfly Porous Fence, Chemical Engineering Transactions, 76, 85-90 DOI:10.3303/CET1976015

2. Butterfly porous fence model and numerical simulation

2.1 Butterfly porous fence model

The structure of butterfly porous fence model was shown in Figure 1. Butterfly porous fence had the porosity of 0.270, the length of 600 mm, the width of 125 mm, the thickness of 1 mm, and the hole of 6 mm.

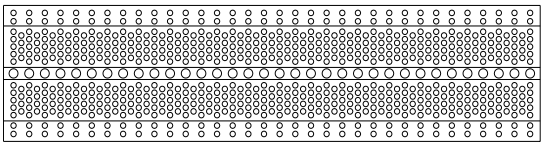

Figure 1: Schematic diagram of butterfly porous fence

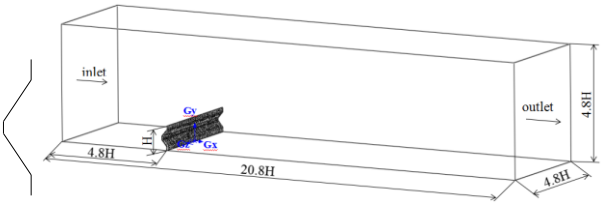

Figure 2: Computational model

Model was established by SOLIDWORKS. Length of the model was 2,600 mm (20.8 H), and size of the cross section was 600 mm (4.8 H) × 600 mm (4.8 H). Butterfly porous fence was placed 600 mm (4.8 H) away from the entrance of the calculation model. The height H (125 mm) of butterfly porous fence was used as the reference for 3D model. It was shown in Figure 2.

2.2 Governing equation

In the ANSYS Fluent, wind was regarded as incompressible fluid, which abides by the conservation of mass, momentum, dissipation rate equation and turbulent flow additional turbulent kinetic energy equation.

2.2.1 Mass conservation equation

$$\frac{\partial u}{\partial x}+\frac{\partial \upsilon}{\partial y}+\frac{\partial \omega}{\partial z}=0 \tag{1}$$

Where u was the velocity in the x direction, υ was the velocity in the y direction, and ω was the velocity in the z direction.

2.2.2 Momentum conservation equation

$$\rho u_j \frac{\partial u_i}{\partial x_j}=\frac{\partial}{\partial x_j}\left[\mu\frac{\partial u_i}{\partial x_j}+\rho C_\mu \frac{k^2}{\varepsilon}\left(\frac{\partial u_i}{\partial x_j}+\frac{\partial u_j}{\partial x_i}\right)-\frac{2}{3}\rho k\delta_{ij}\right]-\frac{\partial p}{\partial x_i} \tag{2}$$

Where ρ was density of gas kg/m^3, u_i was the velocity component in the i direction m/s, u_j was the velocity component in the j direction m/s, x_i was coordinates in the X direction, x_j was coordinates in the Y direction, δ_{ij} was Kronecker tensor, and μ was aerodynamic viscosity coefficient kg/(m·s).

2.2.3 Governing equations for turbulence simulation

Research groups were referred to Giannoulis et al. (2010). The RNG **k-ε** equation used in the simulation was obtained from Hong et al. (2015). Eq(3) in the presented study is equation **k** in the original study, and Eq(4) is equation **ε**.

$$\frac{\partial(\rho k u_i)}{\partial x_i}=\frac{\partial}{\partial x_j}\left[\alpha_\kappa \mu_{\text{eff}}\frac{\partial k}{\partial x_j}\right]+G_\kappa-\rho\varepsilon \tag{3}$$

$$\frac{\partial(\rho \varepsilon u_i)}{\partial x_i}=\frac{\partial}{\partial x_j}\left[\alpha_\varepsilon \mu_{\text{eff}}\frac{\partial \varepsilon}{\partial x_j}\right]+\frac{C^*_{1\varepsilon}}{\kappa}G_\kappa-C_{2\varepsilon}\rho\frac{\varepsilon^2}{\kappa} \tag{4}$$

$$G_\kappa=\mu_t\frac{\partial u_i}{\partial x_j}\left(\frac{\partial u_j}{\partial x_j}+\frac{\partial u_j}{\partial x_i}\right) \tag{5}$$

$$\mu_{eff} = \mu + \mu_t \,,\ \mu_t = \rho C_\mu \kappa^2 \Big/ \varepsilon \,,\ C_{1\varepsilon}^* = C_{1\varepsilon} - \frac{\eta\left(1-\eta/\eta_0\right)}{1+\beta\eta^3} \,,\ \eta = \left(2E_{ij}\bullet E_{ij}\right)^{1/2}\frac{\kappa}{\varepsilon} \,,\ E_{ij} = \frac{1}{2}\left(\frac{\partial u_i}{\partial x_j} + \frac{\partial u_j}{\partial x_i}\right).$$

Where C_μ(0.0845) was selected by experience, G_k was production term of turbulent kinetic energy k (caused by average velocity gradient), α_k (1.39) was Prandtl number corresponding to kinetic energy k, α_ε (1.39) was Prandtl number corresponding to the dissipation rate ε, μ_t was turbulence viscosity coefficient kg/(m·s), η_0 = 4.377 β = 0.012 was coefficient of thermal expansion K^{-1}, $C_{1\varepsilon}$ was turbulence factor, the value was 1.42, $C_{2\varepsilon}$ was turbulence factor, the value was 1.68, and E_{ij} was average rate of change per hour.

2.3 Independence of grid

The number of grids includes: 2,968,686, 3,629,952, 4,847,386, 5,618,815 and 6,139,707. Overall force of the stencil as the grid independence verification index was taken. Overall force of the butterfly porous fence decreases with the increase of the number of grids. The difference of the butterfly porous fence overall force was only 0.11 between the grids number of 5,618,815 and the grids number of 6,139,707. The number of computational grids was determined to be 5,618,815 without affecting the simulation.

2.4 Simulation condition setting

The simulation chose pressure-based discrete solution method in the solver. The calculation accuracy was set to 10^{-5}, the solution method adopted SIMPLEC algorithm, and the calculation method was steady calculation. The boundary conditions were shown in Table 1.

Table 1: Boundary conditions

Boundary condition type	Setting conditions
Entrance boundary condition	Speed entry, exponential function
Export boundary conditions	Free flow, full development
Top side, two sides	Zero shear slip wall

3. Results of PIV experiment and numerical simulation

The butterfly porous fence with the porosity of 0.270 had the wind velocity of 4.0 m/s and 10.0 m/s. A distribution diagram of the net flow line was obtained by numerical simulation and PIV experiment in Figure 3. In the Figure 3, the position of the butterfly porous fence was X = 0 mm. X = 100 mm was 100 mm behind the butterfly porous fence. Y = 40 mm meant that the fence height of the butterfly porous fence was 40 mm.

In the Figure 3, the first picture was a numerical simulation of wind speed of 4.0 m/s. The second picture was a PIV of wind speed of 4.0 m/s. The next picture was a numerical simulation of wind speed of 10.0 m/s. The last picture was a PIV of wind speed of 10.0 m/s. Velocity distribution of the numerical simulation was the same as the velocity distribution of the PIV in Figure 3. The streamline distribution was basically the same in the trend. The wind speed in the top area of the butterfly porous fence was higher than that in the rest area. Therefore, there was a high wind speed area. The section of the butterfly porous fence was uneven. There was low wind speed area with vortex shedding. It was accompanied by some vortices near the fence height of the butterfly porous fence after the wind passed through the butterfly porous fence. Due to the accumulation of tracer particles during wind tunnel experiments, measurement errors may be occurred in PIV. The numerical simulation was different from the PIV far away from the butterfly porous fence.

In order to analyze the difference of numerical simulation and PIV, the value of the velocity distribution in the X direction of the fence height (Y = 125 mm) section were plotted as Figure 4.

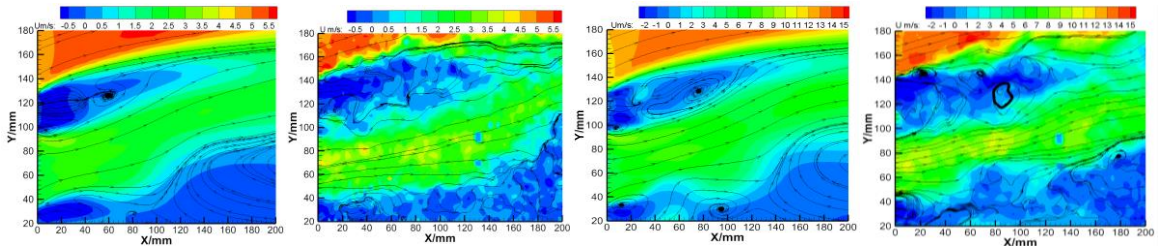

(a) Wind speed 4.0 m/s *(b) Wind speed 10.0 m/s*

Figure 3: Comparison of the streamlines between numerical simulation and PIV after butterfly porous fence at (a) 4.0 m/s (b) 10.0 m/s

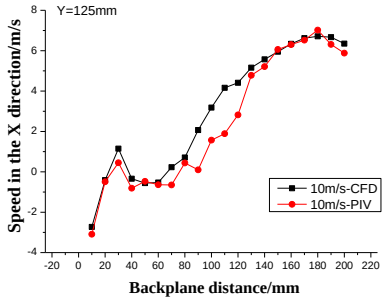

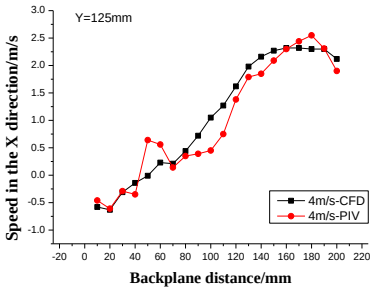

(a)Wind speed 4.0 m/s *(b) Wind speed 10.0 m/s*

Figure 4: Comparison results of numerical simulation and PIV in the Y = 125 mm for wind speed at (a) 4.0 m/s (b) 10.0 m/s

The simulated value of the speed in the X direction on the section of the fence height (Y = 125 mm) was the same as the experimental value in Figure 4. Under the same speed of wind, the numerical simulation of the same position behind the fence was close to the PIV. Their relative error was within 15 %, the minimum relative error was only 1 %, and the average relative error was 20 %. There were some vortices after the wind passed through the butterfly porous fence. In the numerical simulation and the PIV, the X direction velocity of the butterfly porous fence had a negative value. With the increase of distance, the speed in the X direction was from negative to positive. The results of the numerical simulation agreed well with the results of the PIV within the allowable range of error.

4. Results and discussion

4.1 Drag coefficient calculation formula

And worldwide, the wind load calculation formula for porous fence was (6)：

$$F = \frac{1}{2} c_d A_{ref} \rho \upsilon_{ref}^2 \tag{6}$$

This paper defined the drag coefficient by referring to formula (6):

$$c_d = 2\frac{F / A_n}{\rho \upsilon_{ref}^2} \tag{7}$$

Where F was the force N, A_{ref} was the porous fence area on the outer contour m^2, A_n was the porous fence projection area in downwind direction m^2, ρ was the gas density kg/m^3, υ_{ref} was the wind speed at reference height m/s, and c_d was the drag coefficient.

4.2 Effects of wind speed（υ_{ref}）on the drag coefficient（c_d）

Groups chose the butterfly porous fence whose porosity was 0.270 and hole diameter was 6 mm. the values of the wind speed were 3.0 m/s, 5.0 m/s, 7.0 m/s, 10.0 m/s, 12.0 m/s, 15.0 m/s, 18.0 m/s and 22.0 m/s.

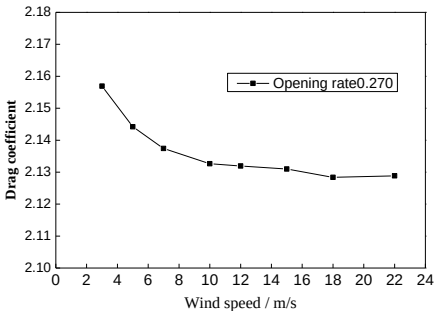

Figure 5: Curves of drag coefficient varying with wind speed

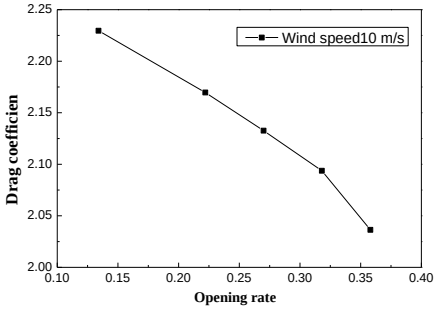

Figure 6: Curves of drag coefficient varying with different open porosity

The drag coefficient of the butterfly porous fence decreases with the increase of wind speed in Figure 5. It was almost unaffected by the change of wind speed. Under the condition of different porosity, the difference value was 0.03 between the maximum drag coefficient and the minimum drag coefficient. The change rate of drag coefficient was only 1.4 %. According to Load code for the design of building structures from the statistics of wind loads in different regions, when the maximum wind speed was over 10.0 m/s, the drag coefficient basically did not change. The drag coefficient of the butterfly porous fence was almost not affected by the change of wind speed.

4.3 Effects of porosity（ϕ）on the drag coefficient（c_d）

In the Figure 6, research groups chose the butterfly porous fence whose hole diameter was 6 mm. It depicted that drag coefficient changed with porosity when the wind speed was 10.0 m/s.
The porosity can be obtained by changing the lateral spacing between the butterfly porous mesh. In order to study the effect of the porosity on the drag coefficient, Butterfly porous fences were designed whose porosity were 0.134, 0.222, 0.270, 0.318 and 0.358. The drag coefficient of the butterfly porous fence was affected by the porosity, and the drag coefficient of the butterfly porous fence decreases gradually with the increase of porosity in Figure 6.

4.4 Drag coefficient formula fitting of the butterfly porous fence

When porosity was 0 ~ 0.367 at different hole diameters, the followings were the fitting formula for the numerical simulation of the butterfly porous fence drag coefficient:
(1) When the hole diameter was 6.6 mm: (Correlation coefficient: $R^2 = 0.996$)

$$c_d = -0.448\phi + 2.280 \tag{8}$$

(2) When the hole diameter was 7.4 mm: (Correlation coefficient: $R^2 = 0.991$)

$$c_d = -0.624\phi + 2.283 \tag{9}$$

(3) When the hole diameter was 8.1 mm: (Correlation coefficient: $R^2 = 0.996$)

$$c_d = -0.702\phi + 2.281 \tag{10}$$

(4) When the hole diameter was 8.6 mm: (Correlation coefficient: $R^2 = 0.998$)

$$c_d = -0.768\phi + 2.282 \tag{11}$$

(5) When the hole diameter was 9.5 mm: (Correlation coefficient: $R^2 = 0.997$)

$$c_d = -0.870\phi + 2.274 \tag{12}$$

By analyzing the formula (8) ~ (12), it can be summarized as a general type.

$$c_d = k\phi + 2.280 \tag{13}$$

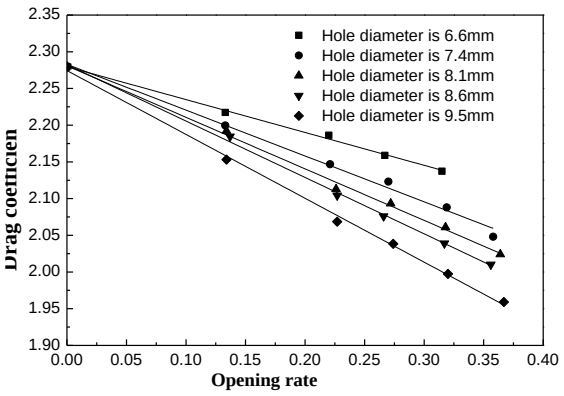

Figure 7: Changing curve of butterfly porous fence of drag coefficient at different hole diameters

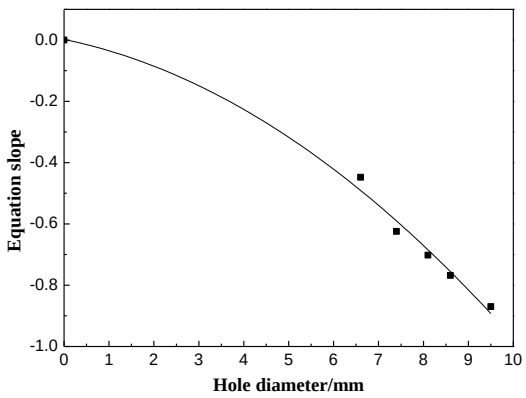

Figure 8: Changing curve slope of fitting equation at different hole diameters

In Eq(13), *k* was the slope of the fitted equation. It could be attributed to the function of the hole diameter.

$$k = f(d) \tag{14}$$

In the Figure 8, the relationship between the slope of the fitted equation and the hole diameter was nonlinear. As the hole diameter increases, the slope of the fitted equation became smaller than before.
When d was 6.6 mm ~ 9.5 mm. (Correlation coefficient: $R^2 = 0.986$)

$$k = 0.00185 - 0.030d - 0.0067d^2 \tag{15}$$

5. Conclusion

This paper aims to study the drag coefficient of butterfly porous fence. The PIV technique is used to compare the PIV of the butterfly porous fence with the numerical simulation. It verified the correction of the numerical simulation and draws the following conclusions：

(1) When the wind load is calculated, the wind speed usually exceeds 10.0 m/s. There was almost no influence on the drag coefficient of the butterfly porous fence.

(2) $\mathbf{C_d}$ and **k** are different for different hole diameters in this paper. When **d** is 6.6 mm ~ 9.5 mm, **k** = 0.00185-0.030 × **d**-0.0067 × $\mathbf{d^2}$.

The correctness of the numerical model are verified through experiments, but the correctness of the formula are not verified with experiments. Consequently, the proposed formula has certain limitations. Future works need to be done to expand the scope of the application of the formula. A critical step is to investigate the features of the porosity and the hole diameter to obtain a more general formula.

Acknowledgments

This paper has been supported by the science and technology of people's livelihood fund project in Qingdao (Research Project: 15-9-2-113-nsh). The national environmental protection atmospheric combined pollution source and control key laboratory open fund project (Research Project: SCAPC201405). The natural science fund project of Shandong Provincial (Research Project: ZR2015DL007).

References

Briassoulis D., Mistriotis A., Giannoulis A., 2010. Wind forces on porous elevated panels. Journal of Wind Engineering and Industrial Aerodynamics, 98, 919 - 928.

Chen G.H., Bai X.H., Li J.L., 2015. Mechanical characteristics analysis of deflector porous fence. CIESC Journal, 66, 3685 - 3691.

Duan Z.Y., Liu Y.Z., Wang K., Zhang Y., Lan Z.J., Xu E.L., 2017. Review of fugitive dust dispersion law from large open-yard of stockpile. Journal of Earth Environment, 8, 307 - 319.

Ferreira A., Lambent R., 2011. Numerical and wind tunnel modeling on the windbreak effectiveness to control the aeolian erosion of conical stockpiles. Environmental Fluid Mechanics, 11, 61 - 76.

Giannoulis A., Mistriotis A., Briassoulis D., 2010. Experimental and numerical investigation of the airflow around a raised permeable panel. Journal of Wind Engineering and Industrial Aerodynamics, 98, 808 - 817.

Hong S.W., Lee I.B., Seo I.H., 2015. Modelling and predicting wind velocity patterns for windbreak fence design. Journal of Wind Engineering and Industrial Aerodynamics, 142, 53 - 64.

Han Z.Z., 2009. FLUENT-example and analysis of fluid engineering simulation (1st Ed.). Beijing Institute of Technology Press, Beijing, PRC.

Xu E.L., Zhou C., Li S.P., Liu Y.Z., Duan Z.Y., 2017. Research on drag coefficient of planar porous fence. Chemical Engineering, 45, 49 - 55.

Xu H.T., Li M.S., Liao H.L., Pu H.L., 2010. Wind tunnel test and determination of structure design parameter for windbreak. Architectural Structure, 40, 104 - 107.

Zhou C., 2017. Computational method study on drag coefficient of porous fence. MSc Dissertation, Qingdao University of Science and Technology, Qingdao, PRC.